BICEP: A Large Angular Scale CMB Polarimeter

Brian G. Keating[a], Peter A. Ade[b], James J. Bock[c], Eric Hivon[d],
William L. Holzapfel[e], Andrew E. Lange[a], Hien Nguyen[b], Ki Won Yoon[a]

[a]California Institute of Technology, Mail Code 59-33, Pasadena, CA, 91125
[b]Dept. of Physics, Cardiff University, Cardiff CF243YB, Wales, UK.
[c]Jet Propulsion Laboratory, 4800 Oak Grove Dr., Pasadena, CA 91109
[d]IPAC, Mail Code 100-22, Pasadena, CA 91125
[e]Dept. of Physics, University of California at Berkeley, Berkeley, CA, 94720

ABSTRACT

We describe the design and expected performance of BICEP, a millimeter wave receiver designed to measure the polarization of the cosmic microwave background. BICEP uses an array of polarization sensitive bolometers operating at 100 and 150 GHz to measure polarized signals over a 20° field of view with $\sim 1°$ resolution. BICEP is designed with particular attention to systematic effects which can potentially degrade the polarimetric fidelity of the observations. BICEP is optimized to detect the faint signature of a primordial gravitational wave background which is a generic prediction of inflationary cosmologies.

Keywords: polarization sensitive bolometers, cosmic microwave background – instrumentation, gravitational wave detection

1. INTRODUCTION AND MOTIVATION

The discovery of the cosmic microwave background (CMB) in 1965 elevated the Big Bang to the status of Standard Cosmological Model. Observations of the CMB have recently produced some of the highest precision measurements in cosmology. Measurements from ground based, balloon and space-borne receivers of the anisotropy of the CMB, combined with constraints on large scale structure, have determined many of the fundamental parameters of the standard cosmological model to the few-percent level.[1] Detection of the linear, "grad-mode" polarization of the CMB has the potential to reduce the uncertainties in several key cosmological parameters to the sub-percent level.[2] Despite this great promise, the values of these parameters do not allow for an unambiguous determination of the fundamental paradigm governing the origins of the universe.

The inflationary paradigm[3] provides a testable hypothesis for the early evolution of the universe. Presently there exists increasing circumstantial evidence for an early epoch of rapid, exponential expansion of the universe during the first $\sim 10^{-38}$ seconds following the initial singularity. Clearly, a convincing model of the universe will only be complete when the underlying evolutionary paradigm is understood.

Inflationary models generically predict a primordial stochastic background of gravitational waves which perturb the metric tensor describing the geometry of the early universe.[4] These perturbations (often described as 'tensor modes') affect the geometry differently than energy density perturbations (often described as 'scalar modes'). A model of inflation is not complete unless it predicts the relative contribution of tensor and scalar modes. The scalar modes are the seeds for large scale structure (galaxy clustering) and these perturbations continue to evolve after the inflationary epoch ends producing CMB temperature and polarization fluctuations on all scales. In contrast, the tensor perturbations do not evolve hydrostatically, and their energy density contribution decreases (redshifts) as the universe expands following inflation. The tensor modes produce CMB temperature and polarization fluctuations only on large angular scales ($> 1°$).

The large angular scale temperature anisotropy measurements by the COBE DMR[5] can only constrain the inflation potential to $V_{\rm infl}) < 3 \times 10^{16}$GeV.[6,7] In order to improve this constraint, which hovers tantalizingly

For further information contact Brian Keating, e-mail: bgk@astro.caltech.edu, phone: 1 626 395 8002

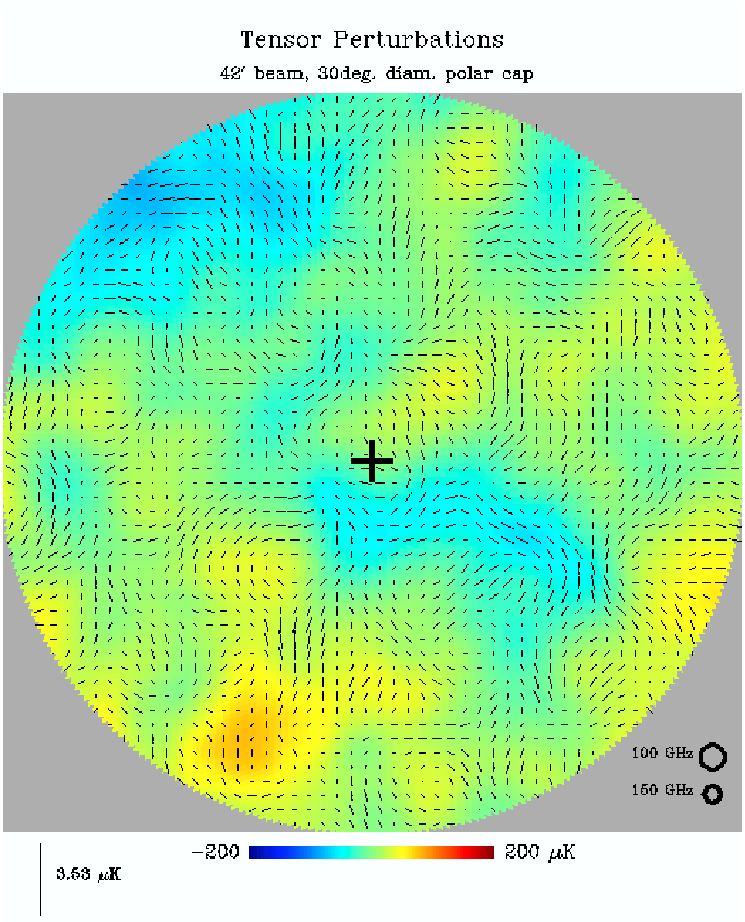

Figure 1. A simulated, 30° diameter, map of the CMB polarization superimposed on the CMB temperature anisotropy (grayscale) around the South Celestial Pole (indicated by cross). The polarization pattern due to tensor modes with T/S = 0.28 (close to the current upper limit) is shown. Since the polarization distribution on the sky is a pseudovector field, it can be decomposed into a zero-curl and a non-zero curl component. Each component is a function of the Stokes parameters Q and U that are used to describe linear polarization. Scalar perturbations produce zero curl component, whereas the GWB produces a field with a non-zero curl component. The fluctuations in temperature and polarization are manifest on large scales and the polarization pattern displays many 'vortices' which indicate regions of non-zero curl. At large angular scales these regions are only generated by tensor perturbations. At smaller scales, gravitational lensing of the grad-mode polarization can produce non-zero curl. Note the large difference between the temperature and polarization scales.

close to the energy scale (10^{15} to 3×10^{16} GeV) characteristic of 'Grand Unified' particle physics theories ("GUT") it is necessary to probe directly for the gravitational wave background (GWB) produced from quantum fluctuations during the inflationary epoch.

Though polarization of the CMB is yet to be detected, the theory of CMB polarization is well-developed (see e.g., Hu & White[8] (1997)). Linear polarization of the CMB is produced via Thomson scattering of a quadrupole intensity anisotropy in the rest frame of the electron. Both scalar and tensor perturbations contribute to the quadrupole anisotropy at the epoch of last scattering ($z \sim 1100$). The scalar component dominates the tensor contribution to CMB polarization by at least an order of magnitude. However, the relative contributions of the scalars and tensors can be discriminated using the vector properties of the polarization field. Figure 1 is a simulation of the temperature and polarization patterns produced by tensor perturbations.

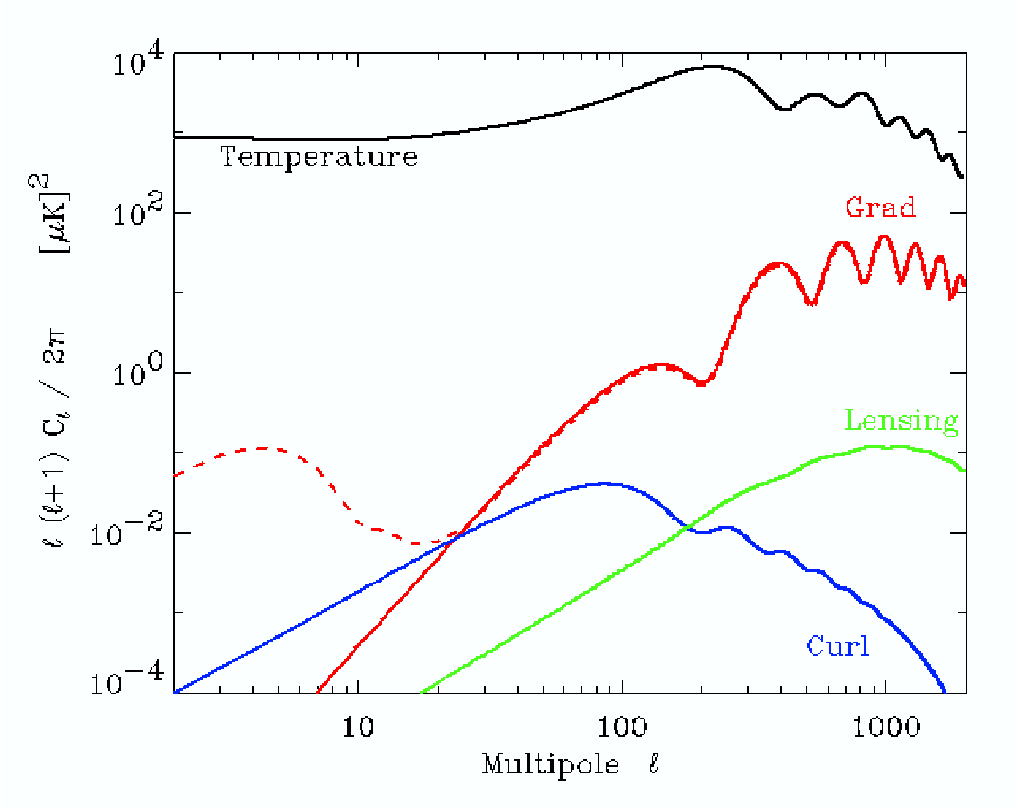

Figure 2. The spatial power spectra of CMB temperature anisotropies (solid), grad polarization (dash), and curl polarization due to the GWB (dotted) and to the lensing of the grad mode (dot-dash), all assuming a standard CDM model with T/S=0.28. Confusion from the curl mode produced by lensing of the grad mode is minimized at $l < 100$.

CMB polarization allows for a unique determination of the source of metric perturbation (tensor or scalar) which therefore provides a direct test of the inflationary paradigm. The perturbation source can be determined directly from the CMB polarization pattern (viewed as a two-dimensional vector field on the celestial sphere). The polarization pattern on the sky can be decomposed into divergence-free and curl-free components in a spherical version of Helmholtz's vector-calculus theorem. Scalar perturbations produce a polarization pattern which can be written as the gradient of a scalar field and tensor perturbations produce a pattern which is the curl of a vector field.[9,10] CMB anisotropy measurements produce scalar maps of the intensity of the CMB and are incapable of directly discriminating the tensor perturbations from the scalar modes.

The amplitude of the curl component of polarization due to the GWB is extremely faint; it will be both difficult to detect and difficult to convincingly distinguish from instrumental, astrophysical and cosmological sources of confusion. Figure 2 shows the relative amplitude of CMB temperature anisotropy, grad-mode polarization, and curl-mode polarization assuming that the amplitude of the GWB corresponds to the current upper limit derived from the COBE DMR. The upper limit of the GWB signature peaks at an angular scale of $\sim 2^\circ$ (multipole moment $\ell \sim 90$), at an rms amplitude of 300 nK (10^{-7} level) corresponding to a tensor-to-scalar ratio of $T/S \simeq 0.5$. Thus, the GWB signature is at least 100 times smaller than the temperature anisotropy.

Theoretical models[11–13]indicate that the fundamental confusion limit on T/S (imposed by gravitational lensing conversion of the grad-mode signal into spurious curl-mode power) is $T/S \simeq 0.001 - 0.01$ corresponding to an inflationary energy scale of $V_{\rm infl} \sim 10^{15}$GeV. While the amplitude of the curl mode power spectrum is unknown, its shape in ℓ-space is robust. This allows for optimization of the experimental angular resolution and necessary sky coverage.[14,15]

It took almost 30 years of effort from the discovery of the CMB until the first clear detection by COBE of

temperature anisotropy at the 10^{-5} level. Fortunately, detector technology has progressed to the point that it is now possible to build a ground-based polarization sensitive receiver which will achieve higher instantaneous sensitivity to the GWB than either MAP or Planck, allowing tensor-to-scalar ratios T/S $\simeq 0.01$ to be probed. Thus, the GUT scale is already within reach of the raw sensitivity of a ground-based receiver deployed to the South Pole. The same technology deployed on orbit would achieve ~ 5 times higher sensitivity still, due to the lower backgrounds.

Though there is a clear path to achieving the necessary raw sensitivity to probe the GUT scale, there is as yet no precedent for accurate polarimetry of any astronomical source at the $\sim 10^{-9}$ level. There is reason to be cautiously optimistic: BOOMERANG succeeded in achieving better than 10^{-6} fidelity[16] by careful design using only a single level of differencing to separate instrumental effects from the signal of interest. BICEP incorporates four levels of differencing, including differences that cleanly separate temperature anisotropy from polarization. Ground-based (as opposed to balloon-borne) experiments will be the most important precursors to a potential future orbital mission (see, e.g.,[17]) since polarization observations are vastly less susceptible to structure in the (unpolarized) emission from the Earth's atmosphere and require vastly more integration time. Experiments sited at the South Pole, which allows extremely long, integration on contiguous regions of the sky[15,18] in very low background conditions, will thus play a uniquely important role in the search for the GWB.

2. INSTRUMENT OVERVIEW

BICEP is designed to measure the curl component of the CMB polarization and particular attention has been devoted to minimizing polarimetric systematics. There are several sources of polarimetric fidelity degradation; most notably: instrumental polarization, cross-polarization and modulation inefficiency. As we will show, the novel and clean optical design of BICEP helps to mitigate all of these effects.

Millimeter-wave radiation enters the instrument through a 200 mm diameter vacuum window, and passes through thermal IR blocking filters at liquid nitrogen (77 K), and helium vapor-cooled (6 K) temperatures. Refracting optics cooled to 4.2 K provide diffraction-limited (Strehl ratio > 0.999) resolution of 1° FWHM at 100 GHz and 0.7° at 150 GHz over the entire 20° instantaneous field of view. A close-packed array of 48 corrugated feedhorns in the 4.2 K focal plane define the beams on the sky and couple the radiation into a solid-state waveguide polarization modulator, described below. The radiation is partially re-collimated by an inverted feed, for transmission to the 0.25 K detector stage. There it is further filtered and coupled to the polarization sensitive detectors via a corrugated feed and waveguide structure.

3. CRYOSTAT

An essential part of BICEP's high final sensitivity to the GWB is the long integration time (comparable to that of satellites) available from the ground. In order to take advantage of the available time, however, the system must run efficiently with a high duty cycle. The cryogenic system is thus designed to be simple, robust, and to use a minimum of liquid cryogens. We have adopted a design similar to that used for the BOOMERANG balloon-borne CMB experiment. The cryostat (Fig. 3) has torroidal tanks in order to house the instrument in a thermally uniform 4.2 K surrounding. The bolometers, optics, ^{3}He refrigerator, and JFETs all mount to an insert that bolts to the bottom of the torroidal ^{4}He tank, in order to allow easy removal for servicing the instrument. Use of a vapor-cooled shield practically eliminates radiated loading from the large window and shields, and conducted loading from wiring onto the liquid helium. We expect the ^{4}He heat load to be dominated by thermal dissipation from the JFET amplifiers and mechanical supports that cannot be thermally shunted to the vapor-cooled shield. The hold time of 25 liters of liquid helium should exceed 4 days under conservative assumptions. The detectors are cooled to 250 mK with a ^{3}He/^{3}He/^{4}He refrigeration system that operates from 4.2 K. A similar system is now in service in ACBAR, and works very reliably.

4. POLARIZATION SENSITIVE BOLOMETERS

Each feedhorn couples to a pair of polarization-selective bolometers (PSBs) that are sensitive to orthogonal linear polarizations. The PSBs have been developed by the Caltech/JPL group for Planck.[19] Aside from the

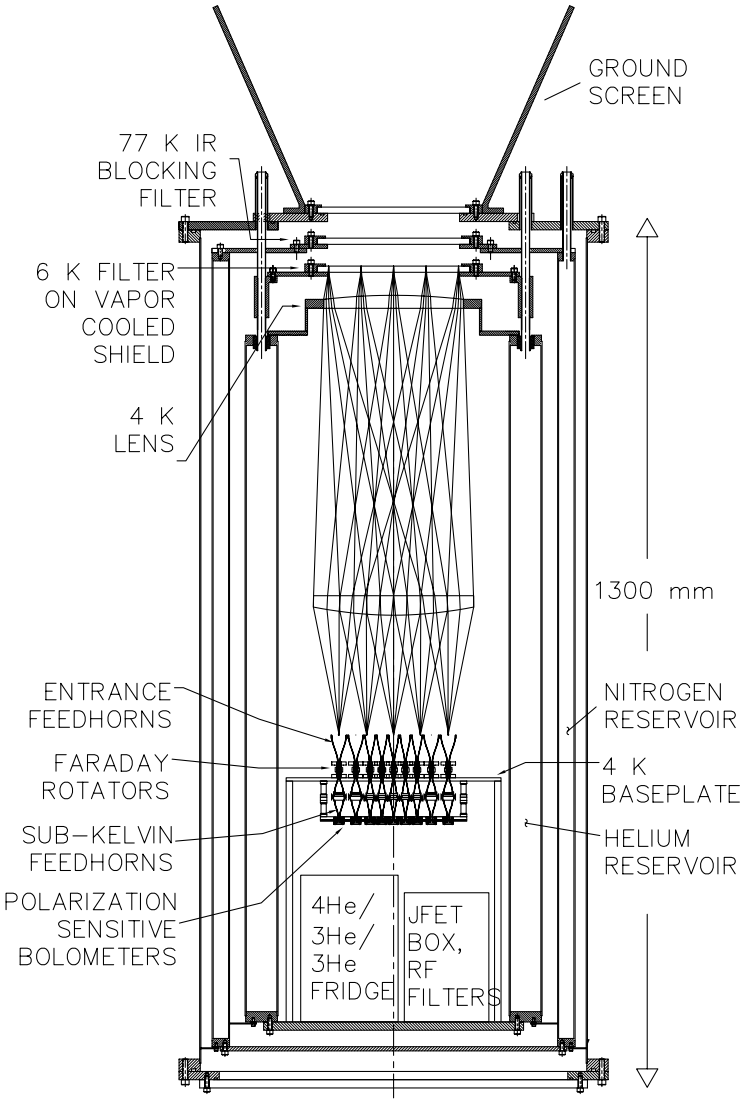

Figure 3. BICEP instrument. See text for complete discussion.

absorber geometry, they are identical in construction and operation to the silicon nitride micromesh ('spider-web') bolometers that are currently in use in ACBAR, ARCHEOPS, BOOMERANG, BOLOCAM and other CMB experiments. In the PSB architecture, the spider-web absorber is replaced with a unidirectional absorbing grid that couples only to a single linear polarization in the guide. A Ge thermistor is located at the edge of the absorber, in a corrugation of the waveguide. Two such detectors, oriented to be sensitive to orthogonal polarizations, are placed in close proximity in the corrugated waveguide and followed by a quarter-wave backshort. The first generation of these detectors have already been fully characterized and integrated into the BOOMERANG cryostat in preparation for flight in late 2002. These detectors reproducibly achieve all of the performance requirements necessary for BICEP, including an end-to-end optical efficiency of $> 30\%$, a cross-polarization of $< 1\%$, and a sensitivity to Stokes Q, referred to the entrance of the receiver, of 370 $\mu\mathrm{K}_{\mathrm{CMB}}\,\mathrm{sec}^{1/2}$. The 96 ($2 \times 48$ feeds) bolometers in BICEP are read out with JFET amplifiers operated at ~ 120 K for optimal noise performance. A silicon nitride membrane suspension, recently developed at JPL for SPIRE, enables the 96

JFETs to be thermally sunk to 4.2 K (and thus positioned very close to the bolometers) with ~ 30 mW power dissipation. The bolometers are AC-biased at ~ 100 Hz to eliminate 1/f noise above ~ 0.01 Hz. Synchronous demodulation of the AC signal provides a sub-audio bandwidth of 0.01 Hz - 20 Hz within which the optical signals can be modulated.

5. OPTICAL DESIGN

The optics of BICEP were designed to provide large field-of-view (FOV) images with $\sim 1^\circ$ resolution at 100 and 150 GHz. Particular attention was paid to minimizing polarized systematic effects and unpolarized optical loading which can decrease the sensitivity of the bolometers. A physical optics study of several wide-field camera configurations was performed in order to obtain a design meeting the specified criteria. Using Zemax Software EE version[20] the cross-polarization and image quality (quantified by Strehl ratio) were computed for three telescope designs: an on-axis Cassegrain, an off-axis Gregorian, and a refractor. While both the Cassegrain and the Gregorian designs are capable of producing cross-polarization levels less than 1% for extreme field angles, neither the Cassegrain nor the Gregorian design could produce a high-fidelity (Strehl ratio $\simeq 1$) over a field of view greater that $\sim 2^\circ$. A refractor telescope (Fig. 3) was designed employing two cold (4 K), 20 cm aperture lenses.

Table 1. Physical optics cross-polarization, Strehl ratio and transmission efficiency predictions for BICEP. Perfect coating refers to the ideal coating for fused silica, imperfect coating refers to a coating with refractive index 10% higher than ideal. Dielectric loss is ignored for these calculations. Cross-polarization is quantified by illuminating the system with radiation 100% plane-polarized along one axis and measuring the response along the orthogonal axis.

Frequency	Field Angle	Coating	Cross-Polarization	Strehl Ratio	Transmission Efficiency
100 GHz	0°	Perfect	5.5×10^{-6}	0.9999	0.99989
100 GHz	$\pm 5^\circ$	Perfect	1.1×10^{-5}	0.9995	0.99971
100 GHz	$\pm 10^\circ$	Perfect	1.4×10^{-4}	0.9997	0.99677
100 GHz	0°	Imperfect	6.9×10^{-6}	0.9999	0.92854
100 GHz	$\pm 5^\circ$	Imperfect	4.7×10^{-5}	0.9995	0.92958
100 GHz	$\pm 10^\circ$	Imperfect	3.5×10^{-5}	0.9997	0.93076
150 GHz	$\pm 0^\circ$	Perfect	5.5×10^{-6}	0.9997	0.99993
150 GHz	$\pm 5^\circ$	Perfect	4.8×10^{-5}	0.9989	0.99968
150 GHz	$\pm 10^\circ$	Perfect	8.9×10^{-5}	0.9909	0.99775
150 GHz	$\pm 0^\circ$	Imperfect	7.1×10^{-6}	0.9997	0.98139
150 GHz	$\pm 5^\circ$	Imperfect	5.6×10^{-5}	0.9989	0.98179
150 GHz	$\pm 10^\circ$	Imperfect	1.2×10^{-4}	0.9909	0.98157

BICEP's refractive optics provide Strehl ratios near unity, with cross-polarization levels less than 0.1% across a 20° FOV (Table 1). Achieving low cross-polarization and high optical efficiency depends critically on the anti-reflection (AR) coating. We have developed graded index AR coatings that provide less than 2% loss (dielectric plus reflection) in two 30% bands centered at 100 and 150 GHz when used with Z-cut crystal quartz. Unfortunately, crystal quartz blanks suitable for use as lenses and windows are prohibitively expensive in diameters larger than ~ 4 inches. We have obtained fused silica samples with measured dielectric loss tangents of 2.8×10^{-4}.[21] This material is available in diameters suitable for BICEP's lenses and vacuum window and we expect our AR coating technology will provide reflection coefficients less than 1% per surface.

The refracting optics provide a flat telecentric focal plane simplifying alignment of the optics. The second lens defines the pupil stop, which is surrounded by a black 4.2 K surface. The windows and 77 K optics are

oversized. The edge of the pupil stop is illuminated at < -20 dB and apodized to provide > 100 dB sidelobe rejection at 40° off-axis. The optical polarization is zero at the center of the field, due to the symmetric optics. We estimate that polarized reflection introduces an instrumental polarization of $< 1\%$ at the edge of the 20° field-of-view.

The focal plane f-number (f/2.3) was chosen to couple to an array of corrugated scalar feed horns in a compact, high efficiency design. The array size was chosen to maximally utilize focal plane area with high aperture efficiency.[22] Corrugated feed horns provide both low sidelobe response and intrinsically low cross-polarization.[23] BICEP uses three horns: an entrance feed defines the illumination on the array lens (and therefore on the sky), a second feed attached to the entrance feed couples to the bolometer feed and provides a thermal. The second feed (at 4 K) and the bolometer feed (at 300 mK) are outfitted with resonant metal mesh low-pass filters.[24] Between the two back-to-back feeds there is a high-pass choke section of single (hybrid) mode waveguide. This design is similar to that used in the Planck Surveyor High Frequency Instrument,[25] with the exception that a Faraday polarization modulator (Section 6) is inserted in the single-mode throat section between the two back-to-back feeds.

6. POLARIZATION MODULATION

The faintness of the polarization signal demands exquisite control of instrumental offsets. There are two ways to control offsets: 1) minimize the amplitude of the offset and 2) modulate ("Dicke switch") fast enough to eliminate the effects of fluctuations in the offset. BICEP does both. A balanced, AC-biased bridge readout produces a stable (first) difference signal with 20 Hz bandwidth that is null for an unpolarized input. Operating matched detectors in a null-bridge eliminates common-mode signals due to atmospheric noise, instrumental temperature fluctuations and EMI. The offset magnitude is further minimized by the unobstructed and maximally symmetric optical design. The non-zero signal due to a polarized input is modulated (second difference) at ~ 10 Hz by Faraday rotation of the incoming radiation. The Faraday rotator, illustrated in Figure 4, is similar in function to a rotating birefringent half-waveplate but has no moving parts. It can thus be cooled to reduce loss without the reliability and microphonic problems associated with cooled mechanisms. The Faraday rotator is positioned in the waveguide directly behind the 4.2 K feedhorn. A solenoid wound around the waveguide drives the ferrite into saturation, alternately parallel and anti-parallel to the direction of the incoming radiation. The length of the ferrite is chosen such that the linear polarization is switched through $\pm 45°$.

7. EXPECTED INSTRUMENTAL SENSITIVITY

The sensitivity of the detector system is fundamentally limited by statistical fluctuations in the radiative background on the detectors. We include both photon shot noise ($\mathrm{NEP_{shot}} = (2\mathrm{h}\nu\mathrm{Q})^{1/2}$) and Bose-Einstein photon bunching ($\mathrm{NEP_{B-E}} = (2\eta\epsilon\mathrm{kTQ}/\Delta\nu)^{1/2}$), where Q is the power absorbed at the bolometer.[26] For ground-based experiments where both the instrument optical efficiency η and the emissivity ϵ from the atmosphere and optics may be large, the photon bunching noise can dominate. In this limit, the sensitivity goes as ϵ, not as $\epsilon^{1/2}$. BICEP cools all optics to minimize instrumental emission to take advantage of the low atmospheric loading at the South Pole. These estimates are borne out by the measured sensitivity ($250\,\mu$K sec$^{1/2}$) achieved with ACBAR at 150 GHz. Taking into account the reduction in signal due to coupling only to a single polarization and the decrease in background relative to ACBAR due to the cooled optics, we calculate the sensitivity of each detector (one arm of the PSB pair) to be $370\,\mu\mathrm{Ksec}^{1/2}$ at 100 GHz and $270\,\mu\mathrm{K\,sec}^{1/2}$ at 150 GHz. With 48 feeds (96 detectors) in the focal plane, the system NET is $< 30\,\mu\mathrm{K\,sec}^{1/2}$.

8. OBSERVATIONS, SYSTEMATIC EFFECTS AND SCAN STRATEGY

In addition, the observing strategy must be carefully designed to avoid aliasing of the (larger amplitude) grad component in the decomposition of the map.[15] Gravitational lensing of the grad component produces a curl component that will ultimately limit how small a GWB can be detected via the CMB (e.g.,.[11–13] The GWB signal is best distinguished from the lensing signal at larger angular scales ($\ell < 100$), as shown in Figure 2.

The observing strategy is a crucial element of any CMB experiment, and all the more so for an experiment attempting to separate the curl component of the polarization. Because the curl is a faint and intrinsically

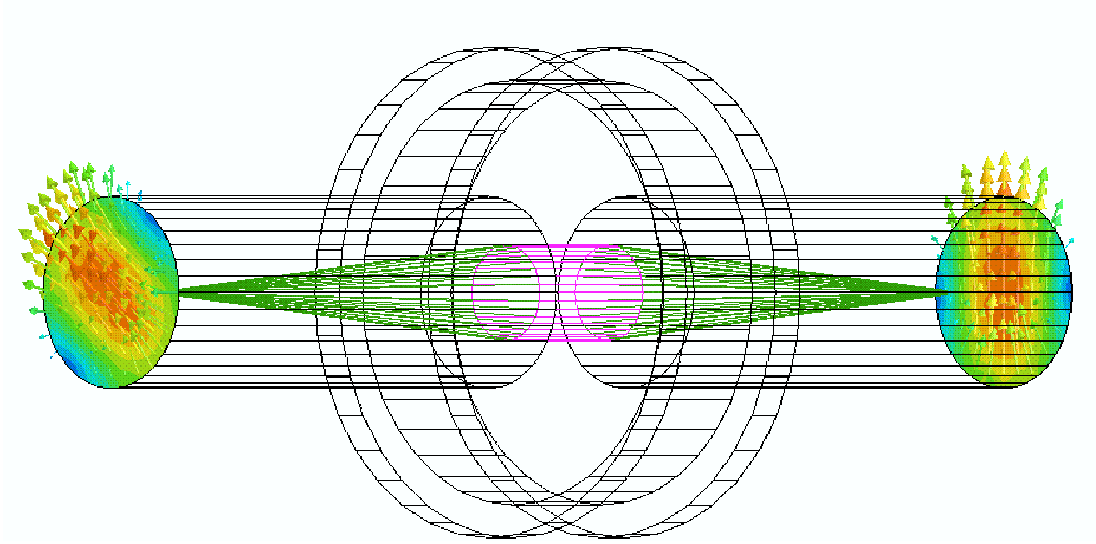

Figure 4. Simulation of a Faraday polarization modulator. A ferrite toothpick is supported between two cylindrical waveguides and surrounded by a superconducting solenoid. The toothpick is approximately one free-space wavelength long, which produces 45° rotation when the ferrite is saturated ($4\pi M_S = 5000\,\mathrm{Oe}$). The ferrite is driven into saturation and the field orientation switches 180° at a frequency of ~ 10 Hz to produce a $\pm 45°$ polarization rotation.

non-local property of the map, the noise covariance matrix of the map must be especially well understood. In addition, edge effects produced by the map shape can significantly degrade curl-mode power spectrum by aliasing grad-mode into (spurious) curl-mode power. The aliasing depends directly on the ratio of the map's boundary to the map's area and is thus minimized for contiguous regions with smooth edges. BICEP will scan the sky (third difference) by continuous rotation about the optical boresite at ~ 1 rpm, keeping the boresite fixed in azimuth and elevation. The continuous rotation will move most of the detectors over most of the map, as shown in Figure 5, on timescales on which drifts in the polarimeter offsets should be small. At 1 rpm, detectors on the outer radius of the focal plane will move $\sim 1°$ FWHM beam on the sky in 1 second. With the boresite pointed at 5° to 25° from the zenith (the range we intend to use), the rotation of the earth will cause the sky to drift (fourth difference) through the leading edge of the scan at a maximum rate of $\sim 0.1°$/minute. Thus each detector in the array will fully sample the entire map in each day of observing. The boresite can be flipped through the zenith to change the azimuth by 180°, thus allowing the same region of the sky to be observed every 12 hours, if desired.

This scan strategy has many advantages. It produces a tightly cross-linked map of an optimally sized region of the sky from every detector on every day. The timescales of the multiple levels of signal modulation cover the entire range of 100 Hz to 1 year. The mount is relatively light and compact making a very effective ground screen easy to implement. Power will be supplied to the cryostat via a slipring. All of the readout electronics necessary to convert the data from the instrument into a single serial data stream (~ 32 kbs) will be located on the cryostat. Data will be transmitted from the rotating cryostat via an IR link positioned at the bottom of the cryostat on the rotation axis of the cryostat.

The instrument and data analysis must be carefully designed to reject the effects of the change in atmospheric emission incident on each detector as it moves across the sky. The scan modulates the column density of atmosphere by between 3% and 15% for boresite zenith angles of 5° to 25°. Though the instrument is carefully designed to reject this common-mode signal, its large amplitude will likely cause some response at the fundamental of the rotation. Qualitative analysis of the common-mode rejection that we can expect indicates that the residual response at the fundamental of the rotation frequency will be similar in magnitude to the scan-periodic signal in the BOOMERANG data due to the pendulation of the payload, which modulated the airmass that BOOMERANG observed through. Since this residual signal will have a reproducible waveform

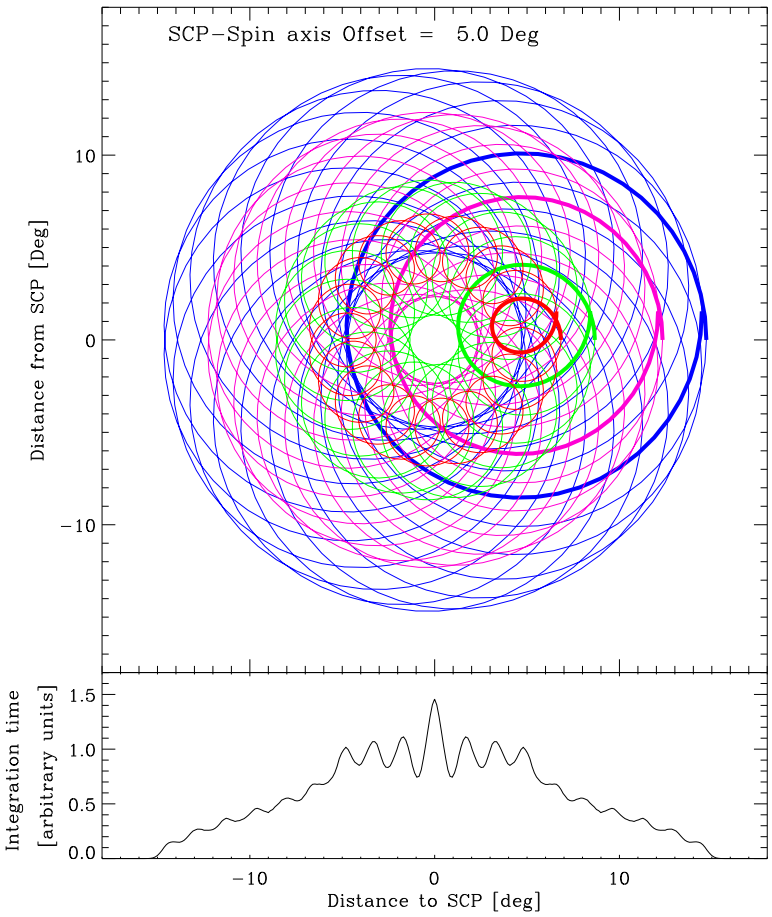

Figure 5. Pixel trajectories and cross-section of map integration times (equivalent to pixel weights) per day for the boresite tipped 5° from the zenith. For clarity. pixel trajectories are shown only for four pixels, while the integration time is shown for the full focal plane. A tip angle of 5° provides relatively uniform map coverage as the sky rotates about the zenith. This minimizes the effect of grad-curl mode conversion. The tapering of the pixel weight towards the edges reduces boundary effects (ringing) in the final power spectrum.

and very low harmonic content, it can be efficiently filtered from the data without significantly degrading the cross-linking in the map. Ultimately, the scan-synchronous atmospheric signal is removed from the map by observation at a variety of boresite angles as the sky rotates about the zenith.

Since the gravitational wave signal is so weak, the feasibility of extracting the curl-mode signature from foreground contamination is of fundamental importance. Unfortunately, little is known about the polarization characteristics of galactic foregrounds in the millimeter. Direct extrapolation of the polarization signal from the foreground intensity distribution requires detailed models of the radiative transport physics which, at present, do not exist. Two types of galactic foreground dominate: synchrotron radiation and thermal dust emission. Neither component has been detected by CMB polarization observations. The spatial correlation between synchrotron intensity and polarization is well known.[27] However, extrapolation of its intensity from $\sim 1-3$ GHz (where the majority of polarization measurements have been performed) to frequencies > 100 GHz (where the CMB dominates) is a speculative endeavor at best. To complicate matters, while the spectrum of thermal dust emission is well-known, its intensity-polarization correlation properties are poorly understood.

Given these concerns, and based on our experience with ACBAR, we have adopted a conservative and flexible two-step approach. The first season of observations with BICEP will utilize a focal plane with 8 feeds

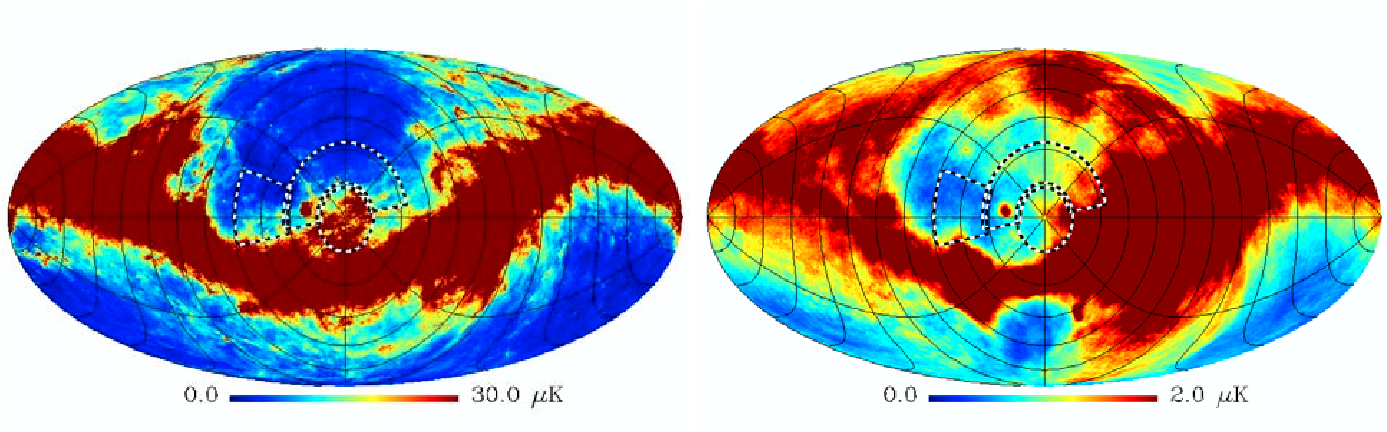

Figure 6. Maps of galactic foregrounds near the South Celestial Pole (SCP). Thermal dust emission (left) is shown based on Finkbeiner, Davis, & Schlegel[28] (1999) extrapolated to 100 GHz. Galactic synchrotron polarization (right) is based on Giardino et al.[29] (2002) extrapolated to 100 GHz using a power law index of -2.8. For both maps, the trapezoid indicates the BOOMERANG field and the circular regions and half-annular regions centered on the SCP indicate the coverage for BICEP.

at each of 100 and 150 GHz (16 feeds, 32 detectors). We will concentrate observations on a 30° diameter circle (boresite at zenith angle 5°) around the SCP until we are limited by foregrounds. In doing so, we will relatively quickly learn enough about the foregrounds to choose how to optimally populate the rest of the focal plane for the next season. We will devote the remaining observations to a half-annular field located at zenith angles between 10° and 30° (boresite at zenith angle 20°), chosen to minimize galactic foreground. Armed with high signal-to-noise maps of selected target regions, the following season we will conduct deep integrations with the fully populated focal plane. The focal plane is designed to be upgraded in the field, a strategy that we have successfully demonstrated with ACBAR.

9. CONCLUSION

BICEP will map $\sim 3\%$ of the sky with 1° resolution at 100 GHz and 0.7° resolution at 150 GHz. BICEP will achieve sensitivity to the gravitational wave background which is comparable to Planck from the ground. Unlike Planck or MAP, it is a true polarimeter, with the ability to rapidly modulate the polarization signal independent of the temperature signal. The South Pole site enables an observing strategy that both minimizes systematics and covers an area of the sky optimized for detection of the GWB.

BICEP is designed to use the polarization of the CMB to constrain the energy scale of inflation at scales typical of the Grand Unified Theory (GUT) scale. Even a null result will begin to probe the universe at a time 10^{-38} seconds after the Big Bang at an energy scale more than 12 orders of magnitude greater than that accessible with current particle accelerators!

ACKNOWLEDGMENTS

BICEP is supported by the Caltech President's Fund, an NSF Astronomy and Astrophysics Postdoctoral Fellowship to B.G.K. and an NSF Graduate Student Fellowship to K.W.Y. We thank Mihail Amarie for performing the optical simulations used in this paper. We are grateful for the generous support of BICEP by the Caltech Discovery Fund.

REFERENCES

1. X. Wang, M. Tegmark, and M. Zaldarriaga, "Is cosmology consistent?," Phys. Rev. D. **65**, p. 123001, 2002.
2. M. Zaldarriaga, D. N. Spergel, and U. Seljak, "Microwave Background Constraints on Cosmological Parameters," *Ap. J.* **488**, pp. 1–+, 1997.

3. A. H. Guth, "Inflationary universe: A possible solution to the horizon and flatness problems," *Phys. Rev. D.* **23**, pp. 347–356, 1981.
4. A. A. Starobinskii, "Cosmic Background Anisotropy Induced by Isotropic Flat-Spectrum Gravitational-Wave Perturbations," *Soviet Astronomy Letters* **11**, p. 133, 1985.
5. G. F. Smoot, C. L. Bennett, A. Kogut, E. L. Wright, J. Aymon, N. W. Boggess, E. S. Cheng, G. de Amici, S. Gulkis, M. G. Hauser, G. Hinshaw, P. D. Jackson, M. Janssen, E. Kaita, T. Kelsall, P. Keegstra, C. Lineweaver, K. Loewenstein, P. Lubin, J. Mather, S. S. Meyer, S. H. Moseley, T. Murdock, L. Rokke, R. F. Silverberg, L. Tenorio, R. Weiss, and D. T. Wilkinson, "Structure in the COBE differential microwave radiometer first-year maps," *Ap. J. Lett.* **396**, pp. L1–LL5, Sept. 1992.
6. J. P. Zibin, D. Scott, and M. White, "Limits on the gravity wave contribution to microwave anisotropies," *Phys. Rev. D.* **60**, p. 123513, 1999.
7. M. Kamionkowski and A. Kosowsky, "The Cosmic Microwave Background and Particle Physics," *Annual Reviews of Nuclear and Particle Science* **49**, pp. 77–123, 1999.
8. W. Hu and M. White, "A CMB polarization primer," *New Astronomy* **2**, pp. 323–344, Sept. 1997.
9. M. Kamionkowski, A. Kosowsky, and A. Stebbins, "Statistics of cosmic microwave background polarization," Phys. Rev. D. **55**, pp. 7368–7388, June 1997.
10. M. Zaldarriaga and U. . Seljak, "All-sky analysis of polarization in the microwave background," Phys. Rev. D. **55**, pp. 1830–1840, Feb. 1997.
11. L. Knox and Y. Song, "A limit on the detectability of the energy scale of inflation," Phys. Rev. D. **89**, p. 011303, 2002.
12. M. Kesden, A. Cooray, and M. Kamionkowski, "Separation of gravitational-wave and cosmic-shear contributions to cosmic microwave background polarization," Phys. Rev. D. **89**, p. 011304, 2002.
13. A. Cooray, "A lensing reconstruction of primordial cosmic microwave background polarization," Phys. Rev. D. **submitted**, pp. astro–ph 0205306, 2002.
14. A. H. Jaffe, M. Kamionkowski, and L. Wang, "Polarization pursuers' guide," Phys. Rev. D. **61**, pp. 83501–+, Apr. 2000.
15. A. Lewis, A. Challinor, and N. Turok, "Analysis of CMB polarization on an incomplete sky," Phys. Rev. D. **65**, pp. 23505–+, Jan. 2002.
16. C. B. Netterfield, P. A. R. Ade, J. J. Bock, J. R. Bond, J. Borrill, A. Boscaleri, K. Coble, C. R. Contaldi, B. P. Crill, P. de Bernardis, P. Farese, K. Ganga, M. Giacometti, E. Hivon, V. V. Hristov, A. Iacoangeli, A. H. Jaffe, W. C. Jones, A. E. Lange, L. Martinis, S. Masi, P. Mason, P. D. Mauskopf, A. Melchiorri, T. Montroy, E. Pascale, F. Piacentini, D. Pogosyan, F. Pongetti, S. Prunet, G. Romeo, J. E. Ruhl, and F. Scaramuzzi, "A Measurement by BOOMERANG of Multiple Peaks in the Angular Power Spectrum of the Cosmic Microwave Background," Ap. J. **571**, pp. 604–614, June 2002.
17. J. B. Peterson, J. E. Carlstrom, E. S. Cheng, M. Kamionkowski, A. E. Lange, M. Seiffert, D. N. Spergel, and A. Stebbins, "Cosmic microwave background observations in the post-planck era," *astro-ph 9907276* , 1999.
18. M. Tegmark and A. de Oliveira-Costa, "How to measure CMB polarization power spectra without losing information," Phys. Rev. D. **64**, pp. 63001–+, Sept. 2001.
19. W. Jones, "These proceedings," 2002.
20. Focus Software Inc., *Zemax EE-version*, P.O. Box 18228, Tucson, Arizona 85731 USA,Tel: (520) 733-0130 Fax: (520) 733-0135, http://www.focus-software.com, 2002.
21. P. Goldsmith, *Quasioptical Systems*, New York, IEEE Press, 1998.
22. M. Griffin, J. Bock, and W. Gear, "The relative performance of filled and feedhorn-coupled focal-plane architectures," Applied Optics **submitted**, pp. astro–ph 0205264, 2002.
23. P. Claricoats and A. Olver, *Corrugated horns for microwave antennas*, London, Peter Peregrinus, 1984.
24. C. Lee, P. Ade, and C. Haynes, "Self supporting filters for compact focal plan designs," in *Proc. submillimetre and far-infrared space instrumentation, 30th ESLAB symposium,* **Estec, Noordwijk, the Netherlands**, 1996.

25. S. Church, B. Philhour, A. Lange, P. Ade, B. Maffei, R. Nartallo-Garcia, and M. Dragovan, "A compact high-efficiency feed structure for cosmic microwave background astronomy at millimeter wavelengths," in *Proc. submillimetre and far-infrared space instrumentation, 30th ESLAB symposium,* **Estec, Noordwijk, the Netherlands**, 1996.
26. J. C. Mather, "Bolometer noise: nonequilibrium thoery," Applied Optics **21**, pp. 1125–1129, Mar. 1982.
27. G. B. Rybicki and A. P. Lightman, *Radiative processes in astrophysics*, New York, Wiley-Interscience, 1979. 393 p., 1979.
28. D. P. Finkbeiner, M. Davis, and D. J. Schlegel, "Extrapolation of Galactic Dust Emission at 100 Microns to Cosmic Microwave Background Radiation Frequencies Using FIRAS," Ap. J. **524**, pp. 867–886, Oct. 1999.
29. G. Giardino, Banday, A.J., Gorski, K.M., Bennett, K., Jonas, J.L., and J. Tauber, "Towards a model of full-sky galactic synchrotron intensity and linear polarisation: a re-analysis of the parkes data," *A&A* **387**, p. 82, 2002.